Nanocomposite coatings based on graphene and siloxane polymers deposited by atmospheric pressure plasma. Application to corrosion protection of steel

Abdessadk Anagri, Alibi Baitukha, Catherine Debiemme-Chouvy, Ivan T. Lucas, Jérôme Pulpytel, Mai Tran, Seyedshayan Tabibian, Farzaneh Arefi-Khonsari

Nanocomposite coatings based on graphene and siloxane polymers deposited by atmospheric pressure plasma. Application to corrosion protection of steel

Abdessadk Anagri, Alibi Baitukha, Catherine Debiemme-Chouvy, Ivan T. Lucas, Jérôme Pulpytel, T.T. Mai Tran, Seyedshayan Tabibian , Farzaneh Arefi-Khonsari*

Laboratoire Interfaces et Systèmes Electrochimiques LISE UMR8235, Sorbonne Université, CNRS, 04 place Jussieu, 75005 Paris (France).
e-mail : farzaneh.arefi@sorbonne-universite.fr
keywords : plasma polymer, graphene nanosheets, composite, corrosion, steel, EIS

Abstract

The present study proposes an alternative eco-friendly method to prepare a thin composite coating based on graphene embedded in siloxane polymers which can be used as application for the corrosion protection of steel. The nanocomposite coatings were elaborated by a dielectric barrier discharge using a nebulized colloidal suspension of graphene nanosheets (GNs) dispersed in hexamethyldisiloxane (HMDSO) used as the precursor for the polymer matrix. After obtaining a stable colloidal solution, it was nebulized into the plasma reactor to form a plasma polymer (pp) coating from HMDSO (ppHMDSO) in which GNs were incorporated (GN@ppHMDSO) on the mild steel substrate. The chemical structure of the hybrid coatings was characterized by X-ray photoelectron spectroscopy and Fourier transform infrared spectrometry. Raman spectra of GNs and GN@ppHMDSO coatings suggest the existence of charge transfer between the GNs and the HMDSO matrix. Furthermore, scanning electron microscopy confirms the synthesis of micro/nanocomposite with a fairly homogeneous dispersion of the GNs in the polymer matrix. The corrosion resistance of the samples was evaluated by electrochemical impedance spectroscopy which showed that the hybrid coatings GN@ppHMDSO deposited by a one-step atmospheric pressure plasma process, presented excellent anticorrosion performance with 99.99% of protection efficiency.

1. Introduction

The protection of metallic surfaces against corrosion is a very crucial problem. Depending on the metal and the environment to which it is exposed to, it is important to design a surface treatment which would present a proper durability of the corrosion protection of metals. During these last decades, the corrosion protection of metals by means of protective coatings has received a major interest. Graphene (G) or graphene oxide (GO), possessing lightweight, being impermeable, inert, wear resistant and mechanically strong is a very good candidate for anti-corrosion coatings. G / GO based nanocomposite have shown a great interest not only for corrosion protection of coatings [1–5] but also for other applications such as sensors for flame detection [6,7], as well as for efficient oil/ water separation [8]. Among the different wet deposition processes used for preparing G/GO, functionalized or not, nanocomposite hybrid coatings reported in the literature, we can cite sol-gel processes [4] , dip coating [6] , nanocasting [3], etc. Dry processes although in general require more sophisticated systems for layer deposition are more environmentally friendly. These include chemical vapor deposition (CVD), pulsed laser deposition (PLD), magnetron sputtering and plasma enhanced chemical vapor deposition (PECVD). Several studies reported on PECVD were dedicated to investigate the corrosion protection by plasma coatings at low and atmospheric pressure [9–16]. The mechanisms of PECVD of organic precursors, also called plasma polymerization have been thoroughly reviewed by many authors [34,35]. They have reported that the mechanisms of plasma polymerization are quite complicated, however they agree that the precursor goes through several fragmentation by the reactive species in the discharge (photons, electrons, ions, metastables, etc.). Depending on the plasma conditions, and in particularly at atmospheric pressure, the fragmentation of the precursor gives rise to several radicals which recombine to form the plasma polymers. The latter are characterized by low molecular weight polymer chains. For example in the case of organosilicon plasma polymers, the maximum reported mass determined by MALDI-ToF was 1670 m/z [36] . Usually plasma polymers are characterized

by very crosslinked structures and this is why very thin layers can give rise to very good barrier properties.

Different strategies of coatings have been reported for corrosion protection from simple dense organic polymer layers [9,13], nanostructured layers [17] to hybrid nanocomposites (NC) ones [18]. The latter is particularly interesting, owing to the synergetic effect combining the properties of the different basic components. The first work on NC coating obtained by a dielectric barrier discharge (DBD) was published in 2009 by Bardon *et al.* [18] in which organosilicon coatings containing aluminum-cerium oxide ($AlCeO_3$) nanoparticles (NPs) were deposited. The authors first of all obtained a stable well dispersed colloidal solution of NPs of $AlCeO_3$ in liquid hexamethyldisiloxane (HMDSO) by adding 3% of ethanol to the solution, which was then sprayed in the discharge. The results show homogeneous hybrid coatings with better corrosion protection properties, *i.e.* two times higher polarization resistance as compared to plasma–deposited HMDSO coatings alone. Later, Dembele and co-workers [19], reported the deposition of TiO_2 nanoparticles dispersed in a matrix obtained from tetramethoxysilane. They also studied the effect of alcohols (pentanol and ethanol) on improving the stability of the dispersed colloidal solution. Then the interest of such hybrid coatings was studied for other areas of application such as electrical conductivity as reported by Uygun *et al.* [20]. Indeed the incorporation of TiO_2 nanoparticles in polypyrrole, polythiophene or polyfuran matrix allowed an increase of the conductivity of the composite coating. For biomedical application, Gherardi and co-workers [21] showed a significant antibacterial activity of the nanocomposite coatings obtained by incorporating silver nanoparticles embedded in plasma polymerized polyacrylic acid matrix.

Several authors [9–13,15] have shown the barrier effect of plasma polymerized HMDSO for corrosion protection of different metallic surfaces (steel and magnesium).

Furthermore Prasai *et al.* [22] reported that thin multilayers of pure graphene grown by CVD on nickel slowed down its corrosion rate by 20 times as compared to the uncoated one. Several papers have reported the beneficial effect of incorporating graphene or graphene oxide sheets in composites to enhance the corrosion properties of metals [3-5, 19–23]. Ramezanzadeh *et al.* [27] developed a nanocomposite coating based on silane with functionalized graphene oxide (fGO), by sol-gel before depositing a 100 μm thick epoxy protective layer. Results reveal that the incorporation of fGO nanosheets into the silane film increased the adhesion of the epoxy layer to the steel and therefore significantly enhanced the corrosion protection performance of the epoxy coatings and reduced cathodic delamination.

The other important condition required to obtain good protective coatings on steel, besides the barrier properties of the coatings is the surface pretreatment which aims at improving the adhesion of the coatings to steel, and removal of organic contaminants of the surface. Grundmeir et *al* [32] reported that oxygen plasma on steel removes the surface carbon contamination and creates a passivated layer by increasing the surface concentration of oxidized Fe. Moreover Arefi *et al.* [13] have shown that a SiOx film deposited without oxygen plasma pretreatment presented a weak adhesion to the steel substrate as compared to the pretreated one for which the values were similar to non-coated steel. Mostly, the surface activation by plasma is performed at low pressure [9,12,13,33] which presents a constraint for industrial applications in addition to its cost. So as explained in section I we have used the arc blown atmospheric pressure plasma for the pretreatment [32].

The main goal of this work is to report, for the first time, the deposition of hybrid NC coating based on graphene nanosheets (GNs) embedded within an organosilicon matrix for corrosion protection of mild steel E24 by aerosol-assisted non-equilibrium atmospheric pressure plasma. First the graphene nanosheets were dispersed in HMDSO liquid precursor and then nebulized through a pneumatic atomizer. The physico-chemical properties of the coatings were

investigated by FT-IR, Raman spectroscopy and XPS, and their morphology by SEM-FEG. The anticorrosive behaviour of the hybrid coatings was studied by electrochemical impedance spectroscopy in an aerated media.

2. Materials and methods

2. 1. Chemicals

Graphene nanosheets with particle-size distribution of (D50) between 7-12 μm and presenting a thickness of 1 to 3 layers were purchased from Xiamen Knano Graphene Technology & CO. HMDSO (≥98%), ethanol (absolute ≥ 99.8%) and sodium sulfate (Na_2SO_4) were purchased from Sigma-Aldrich and used without further purification. Mild steel E24 with the chemical composition reported in Table 1 was purchased from Weber-Metaux.

Table 1. Chemical composition of Mild steel E24 [28]

	Fe	C	Mn	P	S	N	Density (kg/m^3)
Weight (%)	**98.3**	**Max 0.2**	**Max 1.4**	**Max 0.04**	**Max 0.04**	**Max 0.012**	**7800**

2. 2. Experimental details of the deposition process

2. 2.1. Pretreatment of steel surface by atmospheric plasma jet

The surface activation was performed at atmospheric pressure by using an atmospheric plasma jet (APPJ) operating in open air gas. The system used has been described previously [29]. Before the pretreatment the substrates were polished successively with sand papers of 600, 1200 and 2400 grit and sonicated in acetone for 10 *min*. In order to avoid any aging effect on the pretreated substrate surfaces, the substrates were coated immediately after APPJ activation.

2. 2.2. Preparation of the colloidal solution and DBD reactor

The colloidal suspension was prepared by introducing 1*wt*% of GN particles into HMDSO liquid precursor. Less than 10% in weight of ethanol was added to improve the dispersion of GN particles in the liquid precursor which lead to a better homogeneity of the dispersion in the coating. The mixture was sonicated by an ultrasonic homogenizer in the pulsing mode with a duty cycle of *50*% and an applied power of 280 *(W)* for 30 min. After sonification the colloidal suspension presented a good stability several hours without any sedimentation, however the mixture was sonicated systematically before injection into the DBD reactor to avoid any aggregation of GN particles. The nebulization of the colloidal suspension into the DBD reactor was carried out using a homemade atomizer with a recirculation reservoir and an additional inlet for the carrier gas. Fig.1 shows a simplified schematic of the DBD reactor used for the deposition of NC coatings. It consisted of a cylindrical stainless steel tube (1.0 cm external diameter) with a coaxial outer ceramic tube (1.7 cm external diameter) used as an upper high voltage electrode. The lower grounded electrode was a stainless steel plate (10 cm*10 cm) covered with borosilicate glass of the same size and a thickness of 3 mm. The gap between the two electrodes was set to ca. 2 mm. The power was supplied by a "Calvatron SG2" high voltage 44 kHz AC supply. The colloidal solution was atomized in the reactor. Furthermore the chemical precursors were introduced via an additional 3D printed home made diffuser, placed before the plasma zone forming a 45° angle with the substrate holder as shown in Fig.1a, in order to ensure a uniform flow at the exit. The whole DBD system was placed in a closed plexiglass box.

a) **b)**

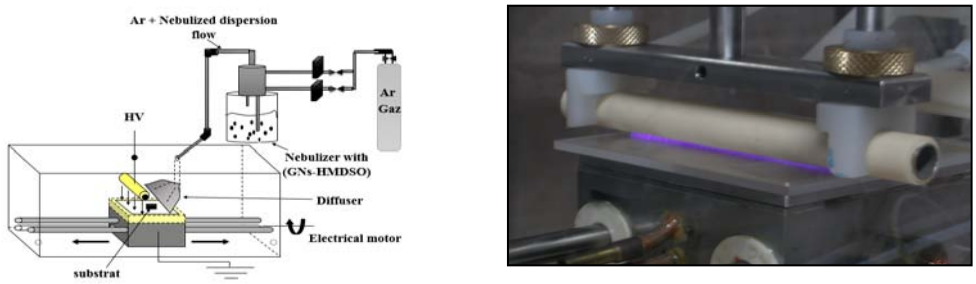

Fig. 1. (a) Schematics of the DBD used for the growth of NC thin film by nebulization of a colloidal suspension of Gr/HMDSO (360.8 µl.min-1 in 8 slpm of argon), (b) Picture showing the plasma discharge.

Fig. 2. Schematics of developed structures

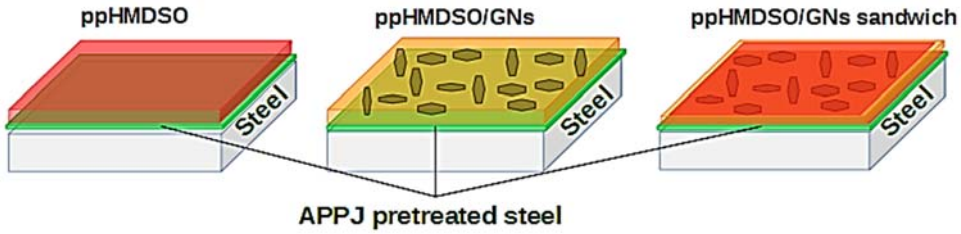

Three structures were deposited by DBD plasma on APPJ-treated steel, (a) pp-HMDSO coatings alone, (b) hybrid layers based on GN@ppHMDSO and (c) a sandwich layer consisting of a hybrid coating of GN@ppHMDSO inserted between two simple layers of ppHMDSO as shown in Fig.2. The total thickness of the protective layers in all cases was kept constant at 500 nm (measured by SEM) by keeping the same number of scans (same time of treatment). In addition to the three above structures shown above, we have studied the corrosion resistance of ppHMDSO coating without pre-treatment.

The electrical characterization of the DBD used for growing the NC coatings was performed by measuring the voltage (kV) and the current (mA) obtained by using a High Voltage GE 3830 probe and a wideband current probe (Pearson Electronics, Inc., model 3972) respectively. The collected signals were recorded by a digital oscilloscope (RSDS 1204 CFL).

Fig.3 shows the electrical characterization of the plasma in the presence of the colloidal suspension of GNs-HMDSO, for an AC voltage at a frequency of 44 kHz and an applied voltage of 7.2 kV peak-to-peak. The signature of the measured current confirms the stability and the homogeneity of the discharge by the presence of two current peaks for each applied voltage period [30,31]. In other words, the presence of the colloidal suspension does not change the electrical signature of the discharge. From both voltage and current curves, the time-averaged electrical power consumed by the plasma DBD reactor can be calculated from the following equation:

$$P = \frac{1}{T}\int_{t=0}^{T} v(\boldsymbol{t}) \text{ x } i(\boldsymbol{t})\, dt \qquad (1)$$

Where v(t) and i(t) are, the voltage and the current versus time respectively, T is the waveform period. The measured power is estimated to be equal to 3.6 W.

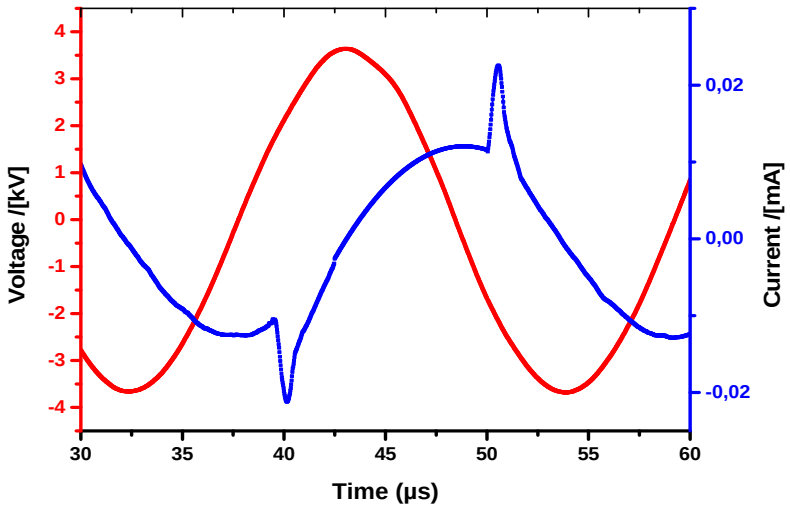

Fig.3. Electrical characterization of HMDSO-GNs in argon gas

2.3. Characterization techniques

Fourier Transform Infrared Spectroscopy (Bruker VERTEX 70 FTIR spectrometer) was used to characterize the chemical structure of the HMDSO and HMDSO-GN coatings. The spectra were acquired at room temperature in transmission mode by depositing the layers on Si (100)

wafers, from 700 to 4000 cm^{-1} with a resolution of 8 cm^{-1}, and a total of 100 scans were recorded for each spectrum.

In order to characterize the vibration and the presence of graphene in the nanocomposite layers, Raman spectra of GN@ppHMDSO coatings on silicon were recorded with a Labram Evolution HR800 microRaman spectrometer (Horiba, Japan) using a 532 nm laser source. The Raman spectra were recorded at room temperature.

X-ray photoelectron spectroscopy (XPS) analyses were carried out on a Thermo Fischer Scientific K-Alpha+ spectrometer using a monochromatic Al Kα X-ray source (1486.6 eV). The survey and the high-resolution spectra were recorded at a pass energy of 150 eV and 40 eV, respectively. A take-off angle of 90° was used for acquiring the spectra. The XPS spectra were fitted using CasaXPS software and Shirley-type background was subtracted.

In order to investigate the morphology of the hybrid coatings, SEM analyses were carried out (SEM-FEG ULTRA 55 ZEISS) on the GN@ppHMDSO hybrid coatings onto silicon substrates. SEM images were acquired in high resolution in-lens secondary electron detector at the working distance of 2 mm, and with an electron accelerating voltage of 15 kV (extra high tension EHT). Before observation the samples with the plasma coatings were sputter-coated with a 5 nm thick layer of graphite.

Electrochemical experiments on mild steel sample were performed by means of GAMRY 600 Potentiostat /Galvanostat. The electrochemical impedance spectroscopy **(**EIS) measurements were carried out with coated (ppHMDSO and GN@pHMDSO) and uncoated mild steel substrates, in 0.5M Na_2SO_4 solution in an aerated cell, using a three-electrode system, where uncoated or coated steel acted as the working electrode. A saturated calomel electrode (SCE, E = 0.24 V/SHE) was used as the reference electrode and a platinum wire was used as the counter electrode. The impedance measurements were performed at open circuit potential

(OCP) in the frequency range of 100 kHz to 0.05 Hz, using an AC amplitude of 10 mV with 10 points per frequency decade.

3. Results and discussion

3.1 X-ray photoelectron spectroscopy

APPJ pretreated mild steel

First of all the surface stoichiometry of the treated sample as compared to non-treated one shows that the pretreatment decontaminates the surface, i.e. the carbon content decreases drastically from 62% to 11%. Furthermore Fig. 4 shows the Fe2p XPS spectra of non-treated and APPJ pretreated steel samples. One can notice that for the untreated steel (spectrum (a)) the Fe(0) contribution at 706.6 eV was detected whereas it was almost absent on the pretreated one (spectrum (b)). These findings clearly confirm that the atmospheric pressure air plasma oxidizes the surface of E24 which leads to: i) a surface cleaning by decontaminating the surface by etching (consumption of carbon in the form of volatile species such as CO and CO_2), and ii) to a thicker passivating layer on steel which can slow down the corrosion on E24 [32].

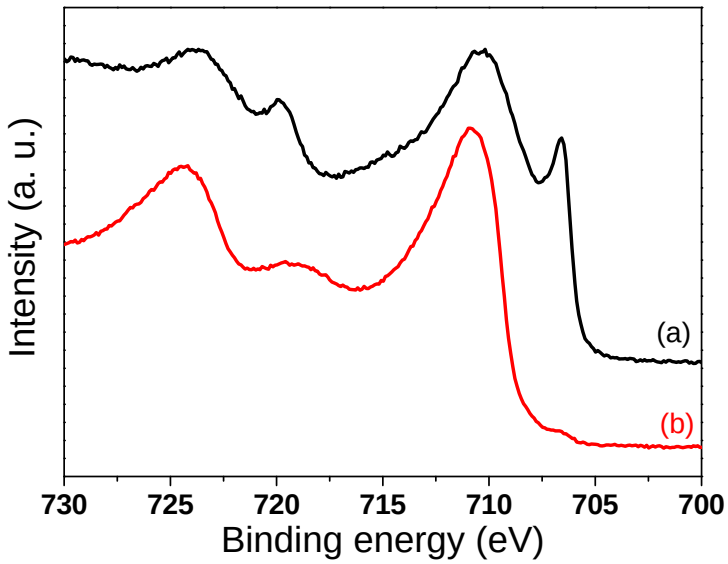

Fig.4. Fe2p photoelectron peak of E24 steel substrates without (a) and with APPJ-air pretreatment (b).

Siloxane and hybrid coatings

An XPS survey of both coatings deposited from pure HMDSO and from the GNs-HMDSO suspension, present silicon, oxygen and carbon elements. The apparent surface elemental composition of pp-HMDSO as well as GNs-HMDSO are fairly the same and are given in Table 2.

Table 2. Surface atomic composition of ppHMDSO and GN@ppHMDSO coatings determined by XPS

	Si (at%)	C (at%)	O (at%)
ppHMDSO	25.1	48.4	26.5
GN@ppHMDSO	25.5	48.0	26.5

The Si2p high resolution spectrum was deconvoluted in Fig.5. O'Hare *et al.*[37,38] investigated siloxane coatings using XPS analysis and proposed a curve-fitting methodology for the Si 2p core level. The same approach based on their results was used to deconvolute the Si $2p_{3/2}$ and Si $2p_{1/2}$ overlapping bands. The Si2p band is fitted with four contributions corresponding to

four different structures in SiO_xC_y films which are given in Table 3. Bearing in mind that in HMDSO molecule each Si atom is surrounded by three methyl groups and one oxygen atom, when the precursor is introduced into the plasma the first fragmentation takes place with the loss of a methyl group because the Si-C bonding is easier to break than the Si-O one. So depending on the experimental conditions either a crosslinked Si-O-Si network is formed, with no carbon or the final polymer contains some methyl groups. This is what can be observed by XPS. So when describing siloxy coating chemistry, a simplified notation is used to represent the number of oxygen atoms attached to the silicon, with an increase in the binding energy each time a methyl group (Me) is replaced by an oxygen atom. The structures considered are: M [$SiMe_3O$], D [$SiMe_2O_2$], T [$SiMeO_3$], and Q [SiO_4], the T and Q structures representing a more crosslinked structure of the coating.

The binding energies given in Table 3 correspond to the Si $2p_{3/2}$ components. For the deconvolution, as explained in references [39,40], the binding energies attributed to the same chemical bonds have been shifted 0.63eV for the $Si2p_{1/2}$ contribution as compared to $Si2p_{3/2}$ ones. In Fig. 5 dotted lines correspond to $Si2p_{1/2}$ contributions while full lines correspond to $Si2p_{3/2}$ ones. . Moreover the area of the $Si2p_{2/3}$ peaks was kept two times higher as compared to $Si2p_{1/2}$ ones.

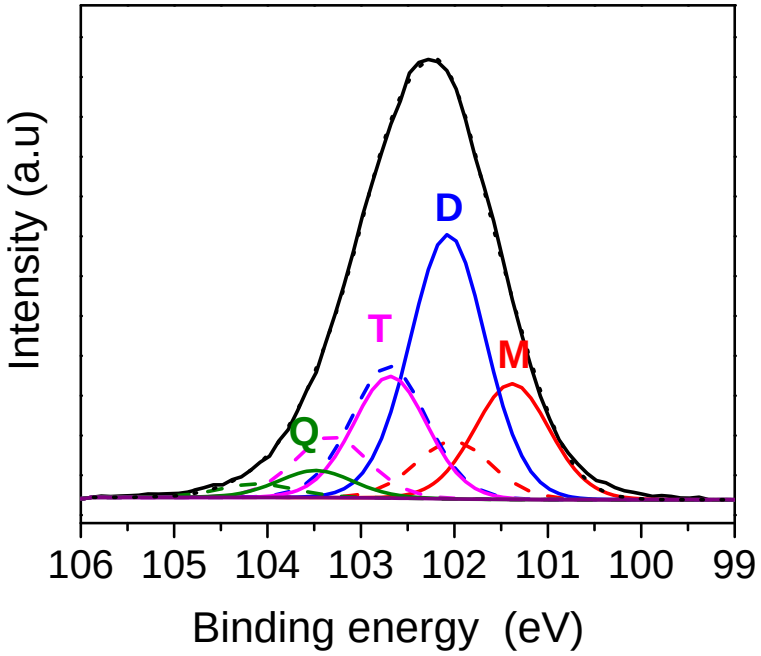

Fig.5. Si 2p XPS deconvolution of ppHMDSO film

Table.3. Si 2p unit structures and their binding energy

	(M) 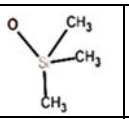	(D) 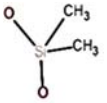	(T) 	(Q) 
Binding energy (eV)	101.4	102.1	102.7	103.5

3.2. Infrared spectroscopy

Fig.6.a presents the FT-IR spectrum of a typical GN@ppHMDSO hybrid coating obtained by the DBD reactor. This spectrum shows a typical absorption feature of amorphous ppHMDSO-plasma (SiCxOy:H) thin film deposited at atmospheric pressure. A large band between 950 and 1250 cm^{-1} corresponding to the asymmetric stretching mode of Si-O-Si with a maximum at 1034 cm^{-1} dominates the spectrum. Between 3250 and 3650 cm^{-1} we note the presence of a wide band related to the vibration of absorbed H_2O, the spectrum shows the presence of organic components, such as the -CH_n vibration in the range of 2900-2970 cm^{-1}, but also the symmetric vibration of Si-CH_3 at 1265 cm^{-1}.

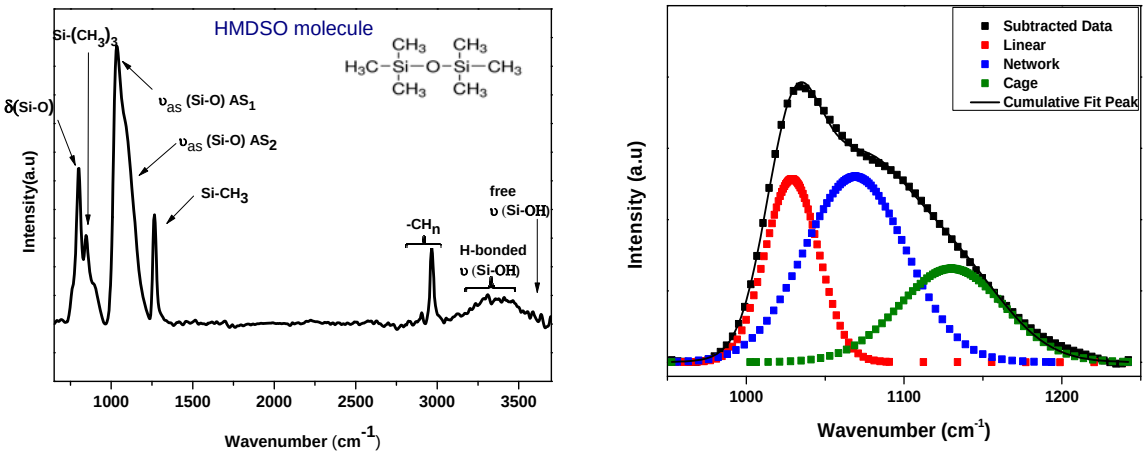

Fig.6. (a) GN@ppHMDSO FT-IR spectrum, (b) Si-O-Si group component deconvolution

As mentioned in the experimental part we have introduced a few weight percentage of graphene in the HMDSO solution. Jiang *et al*[*41*] indicated that there were two theoretical active infrared modes of graphene multilayers: the E_{1u} at 1588.2 cm^{-1} and the A_{2u} at 869.9 cm^{-1}. As for the first vibration in our case no significant signal was observed at this wavenumber considering the fact that a very small percentage of GNs (1%wt) was incorporated into the matrix. As for the second possible energy corresponding to graphene at 869.9 cm^{-1}, it remains difficult to distinguish a peak due to the overlapping with the strong signal of Si-C and Si-O at 840 cm^{-1} and 910 cm^{-1} respectively. Consequently due to the small amount of GNs incorporated into the ppHMDSO matrix we can confirm that there is no significant chemical change in the infrared spectrum.

Gill and Neumayer[39] indicated that for an SiOxCy:H, film the large band of the asymmetric stretching of Si-O-Si can be represented as a sum of three peaks which are centered at 1029, 1069 and 1130 cm^{-1} corresponding to three structures of Si-O-Si namely the linear structure (Si-O-Si), the network structure $Si(-O)_4$ and the cage structure $Si(-O)_3C$. The latter is related to the porosity and the holes in the films as reported by Kim *et al.*[40], indicating a reduction of the density of the silica layer as well as their barrier proprieties. Fig.6.b presents the deconvolution of Si-O-Si by Gaussian fitting, which shows that the films contained a high

percentage of linear and network structure (area =77%) as compared to the cage structure (23%).

By comparing the XPS and FTIR results, we can point out that in terms of the siloxy chemistry of the coatings, these analyses are in fair agreement. Furthermore the fact that 1 wt% GNs has been incorporated in the structure doesn't show any difference in terms of the chemistry of the coatings, as compared to ppHMDSO matrix alone.

3.3. Scanning electron microscopy

SEM observations were performed to study the homogeneity and the size distribution of GNs particles incorporated into the polymer matrix. The obtained micrographs are shown in Fig.7. Clearly the dispersion of graphene nanosheets is fairly homogeneous across the surface. However the GNs have different sizes because of the polydispersity of the graphene used. Using Image J software we analyzed statistically the SEM micrographs of the hybrid coating, Fig.7 illustrates a histogram of the Feret's diameter of GNs embedded into the ppHMDSO matrix. The Feret diameter of particles is between 1 µm to 12 µm, with 80% of the particles ranging between 1 and 7 µm. The mean diameter is 3.5 µm and the most recurrent diameter is around 1 µm. It is worth highlighting that graphene nanosheets are completely or partially covered by the polymer layer, it is also important to specify that the orientation of graphene sheets in the coating is completely random. The Image J was also used to estimate the surface ratio distribution of GNs in the matrix, for 1 wt% of GNs introduced in the HMDSO solution we obtained a surface fraction of GNs of the coated films which was around 1.4 %.

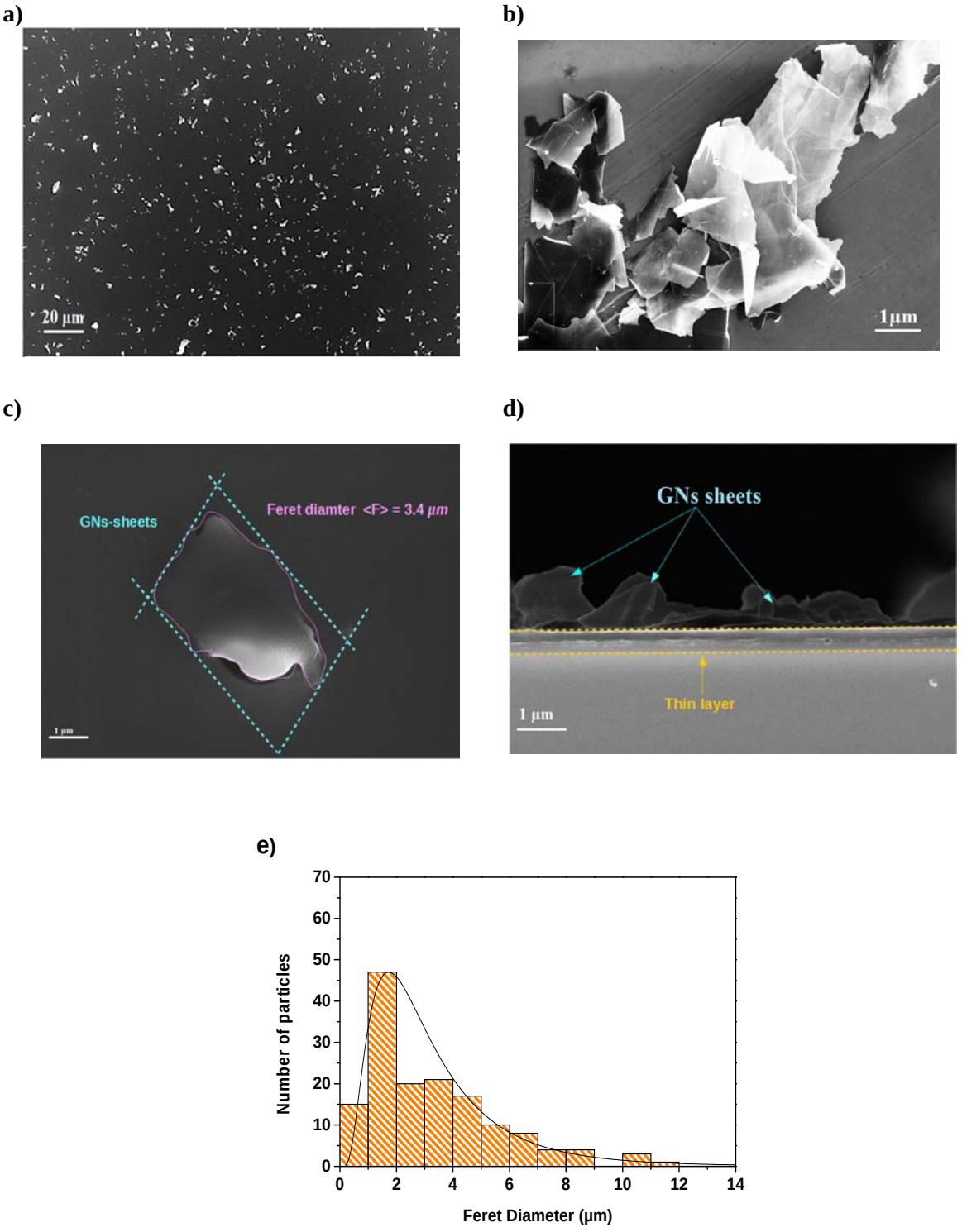

Fig.7. SEM micrographs of (a) and (c) GN@ppHMDSO hybrid, (b) graphene sheets and (e) GNs particles size distribution in ppHMDSO matrix coating

3.4. Raman spectroscopy

Fig.8.a presents the Raman spectrum of pure graphene nanosheets (analyzed as received) and the GN@ppHMDSO coating deposited on a silicon wafer cleaned with ethanol. GNs Raman

spectrum shows three important actives modes, the D mode at 1356.8 cm^{-1} associated to a disordered structured and the presence of defects in the graphene nanosheets, the G mode at 1584.1 cm^{-1} corresponding to the in-plane bonding stretching signal of sp^2 carbon atoms, and the 2D mode at 2723.3 cm^{-1} corresponding to a two-phonon second-order process. In agreement with SEM micrographs presented in Fig.6.b and from the Raman analysis of the GNs, one can conclude that it is a multi-layered graphene [42]. For the GN@ppHMDSO spectrum, in addition to D, G and 2D modes due to the incorporated graphene in the hybrid structure are present, one can notice the presence of two extra peaks at 2909 and 2969 cm^{-1} which can be assigned to the C-H stretching vibrations of the methyl- and methylene groups of the ppHMDSO matrix [43]. A magnification of the G band in Fig.8.b reveals its shift (5 cm^{-1}) to lower frequencies observed for GN@ppHMDSO as compared to graphene nanosheets. As reported by Ghosh *et al.* [44] the G band shift to lower or higher frequencies depends on the nature of electron-donor or electron-acceptor molecules, respectively. This small shift can therefore confirm the existence of a charge transfer between graphene nanosheets and ppHMDSO matrix in the hybrid coating. Based on the similar shape of the spectra of graphene and graphene hybrid coatings, and the minor differences between the two spectra, this could indicate that the plasma does not modify the crystalline structure of graphene introduced into the discharge, which is plausible since it is a high reactive but low temperature plasma. These results also confirm that graphene has not been oxidized to GO upon DBD.

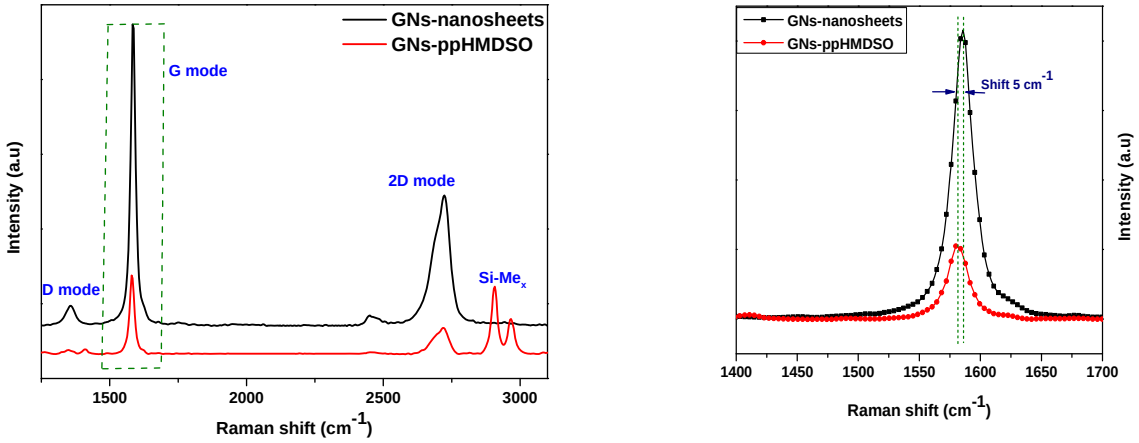

Fig.8. (a) Raman analysis of the GNs and GN@ppHMDSO hybrid coating, (b) focus on the 1500-1700 cm^{-1} region

3.5. EIS analysis of hybrid coatings

Electrochemical impedance spectroscopy was used to compare the corrosion protection of different coatings. Besides the hybrid coatings which were prepared from the nebulization of the stable colloidal solution of HMDSO and 1 wt% of graphene, sandwich structures were prepared in which the hybrid coating was inserted between two simple ppHMDSO layers (without graphene). As explained before, the total thickness of the simple hybrid structure and the sandwich one was similar (verified by SEM). After 24 h of immersion in a 0.5 M Na_2SO_4 aqueous solution, impedance measurements were performed on steel sample pretreated and coated with (i) a ppHMDSO coating without graphene, (ii) a GN@ppHMDSO NC coating, and (iii) a sandwich structure. The results were compared to those of the bare steel. Figs. 9 b, c present the Bode diagrams obtained for the different coatings, in the frequency range of 100 kHz to 0.05 Hz. All the coatings present similar shapes, however the incorporation of GNs into the ppHMDSO matrix leads to a considerable increase of the impedance diagram size thus reflecting a significant improvement of the corrosion resistance of the steel surface. Moreover the hybrid NC coatings deposited in the sandwich configuration appears to show a higher corrosion resistance Table 4 reported the charge transfer resistance values obtained for the

different coatings. Fig. 9c shows the plot of the phase angle in function of the frequency. For high frequencies, we note that for all the coatings, as compared to the uncoated steel, the phase angle decreases from ~ (-90°) to 0°. Moreover after 24 hours of immersion both sandwich and simple hybrid NC coatings show a higher phase angle as compared to ppHMDSO coating, indicating lower coating delamination. This confirms the important role of the interfacial bonding between the coating and substrate. The results confirm that the air plasma activation leads to a good adhesion between the substrate and the nanocomposite coating layer.

According to the Nyquist **Fig. 9, a** and Bode **Figs. 9, b and c** presentations, all coatings presented two capacitive loops which account for two different time constants. The first loop observed at high frequencies is related to the properties of the layer and the second one located at low frequencies could be characteristic of the reactions occurring at the bottom of the coating pores[45]. Hence the experimental data are fitted by considering a simple equivalent circuit, similar to the one used for an electrode coated with an inert porous layer [46] as shown in **Fig. 9 d** , where R_e, R_C, CPE_C, CPE_{dl} and R_t are the electrolyte resistance, layer resistance, constant phase element (CPE) of the layer, constant phase element (CPE) of the double layer and the charge transfer resistance, respectively. Because of the deviation of the coating from the ideal capacitance behaviour, the CPE_C and CPE_{dl} are respectively substituted for the layer capacitance and double layer capacitance to better fitting of the measured EIS data.

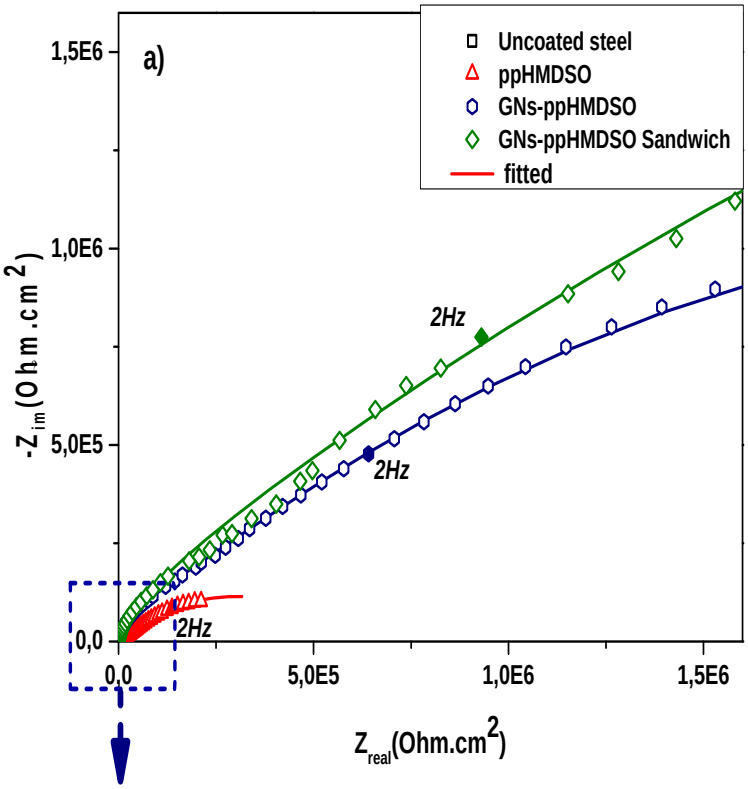
a)
Uncoated steel
ppHMDSO
GNs-ppHMDSO
GNs-ppHMDSO Sandwich
fitted
2Hz
2Hz
2Hz
1,5E6
1,0E6
5,0E5
0,0
0,0
5,0E5
1,0E6
1,5E6
-Z_im(Ohm.cm^2)
Z_real(Ohm.cm^2)

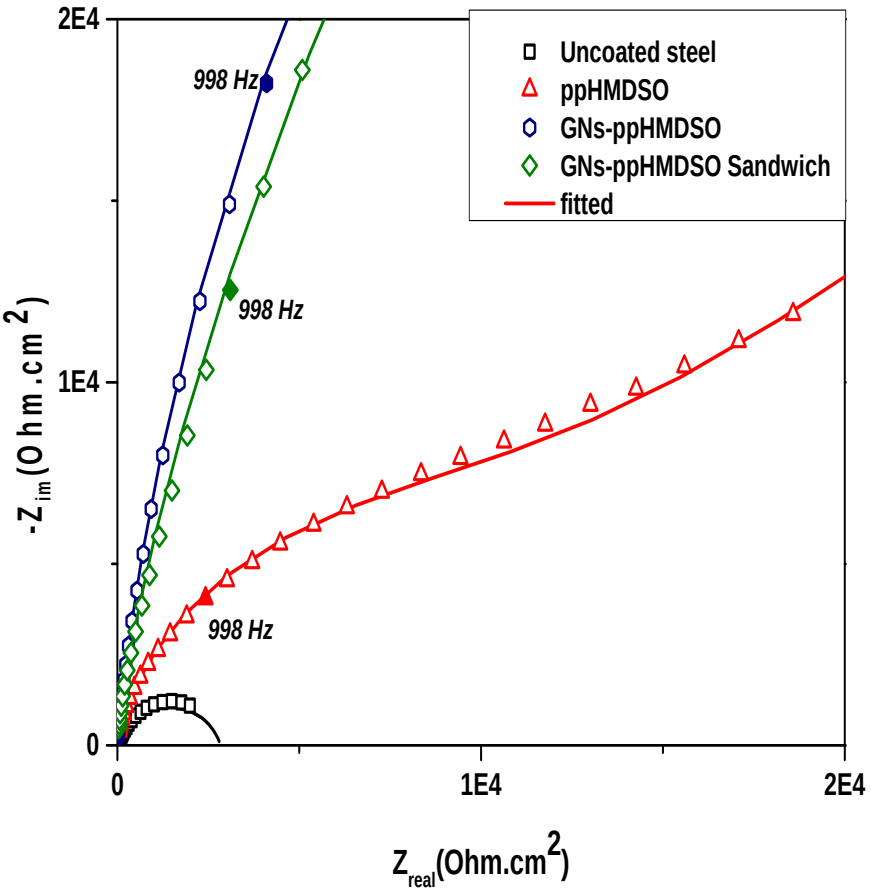
2E4
1E4
0
0
1E4
2E4
998 Hz
998 Hz
998 Hz
Uncoated steel
ppHMDSO
GNs-ppHMDSO
GNs-ppHMDSO Sandwich
fitted
-Z im (O h m .c m 2)
Z real(Ohm.cm2)

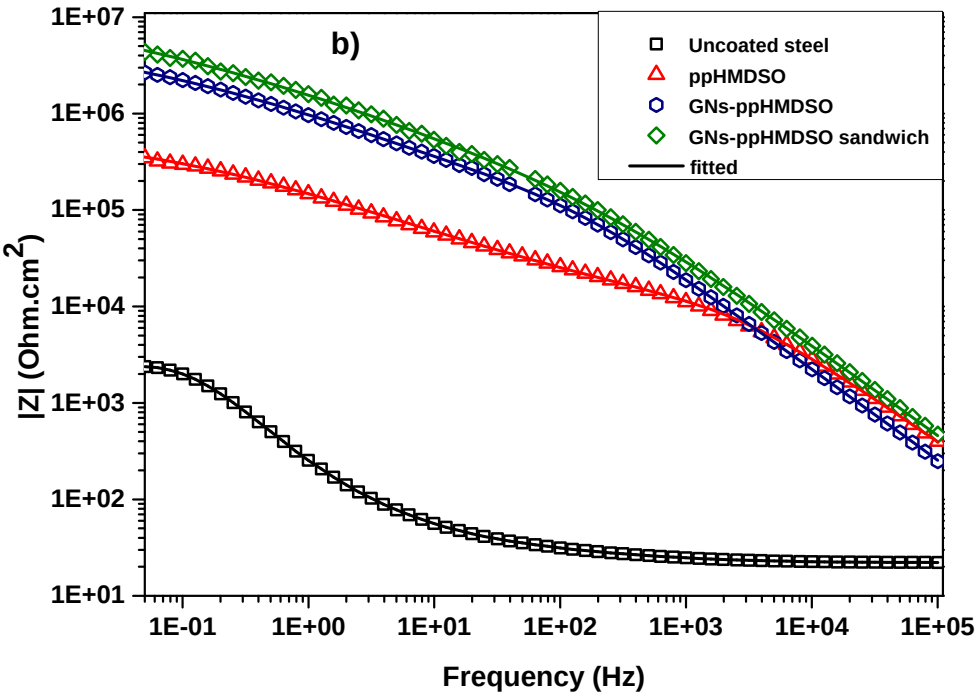
b)
1E+07
1E+06
1E+05
1E+04
1E+03
1E+02
1E+01
1E-01
1E+00
1E+01
1E+02
1E+03
1E+04
1E+05
Uncoated steel
ppHMDSO
GNs-ppHMDSO
GNs-ppHMDSO sandwich
fitted
|Z| (Ohm.cm2)
Frequency (Hz)

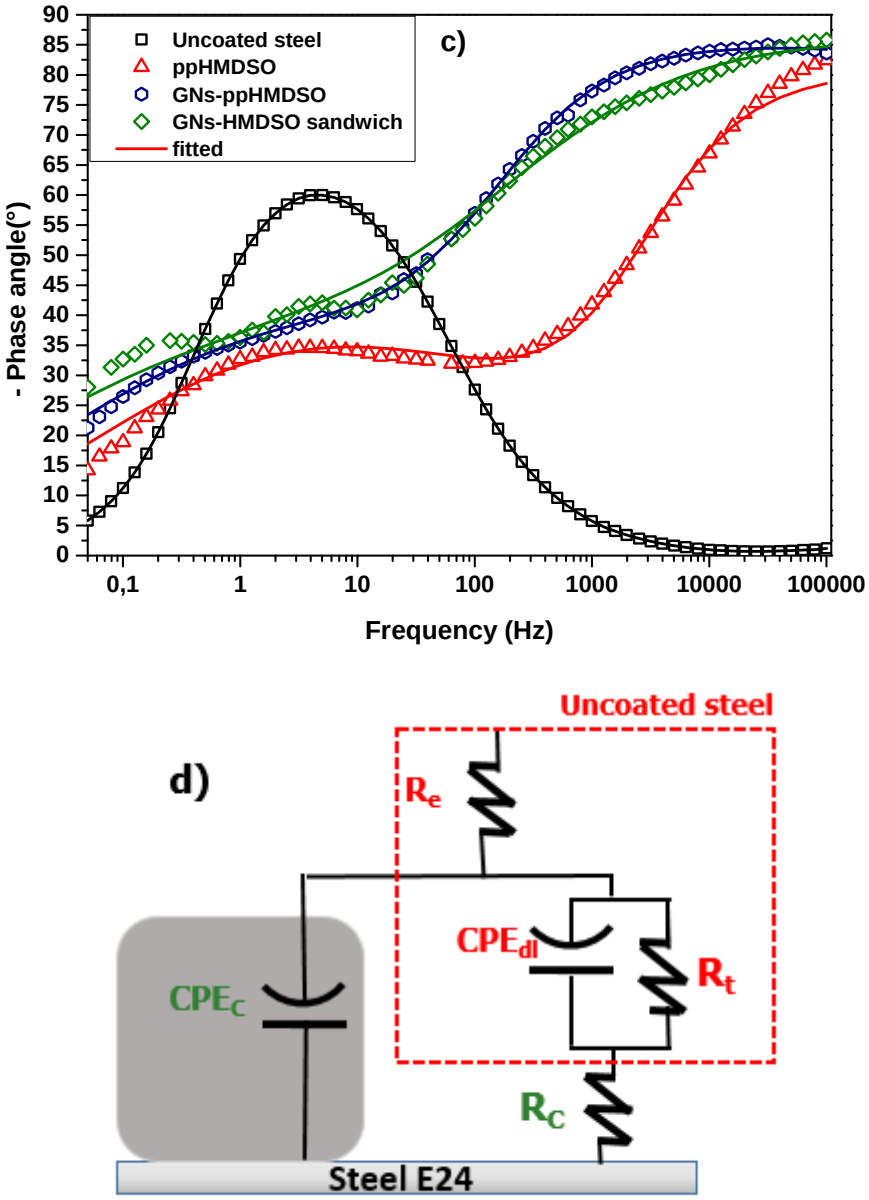

Fig. 9. Nyquist plots (a), Bode diagrams (b), (c) obtained from EIS analysis and equivalent circuit (d) of plasma coated and uncoated steel [46]

The parameter used to estimate the protection efficiency τ (%) for different layers is calculated from equation ***2***. Furthermore, if we consider two hypotheses, i.e. that the pores cross the whole thickness of the coatings and that the corrosion reaction takes place at the bottom of the pores where the electrolyte is in contact with the metal, then, based on EIS measurements under open-

circuit conditions [47-49], we can estimate according to equation 3 the porosity ratio which is the ratio of the charge transfer resistance of the coated steel $R_{t,}$ as compared to that of the uncoated one $R_{t,0}$.

$$\tau = 100*(R_t - R_{t,0})/ R_t \quad (2)$$

$$\text{Porosity ratio} = 100* (R_{t,0} / R_t) \quad (3)$$

The different results are collected in Table 4. This table also reports open circuit potential (OCP) values.

Table.4. Open circuit potential (OCP), charge transfer resistance (R_t), protection efficiency τ(%) and the porosity ratio estimated based on electrochemical impedance spectroscopy measurements.

	OCP (mV/SCE)	Charge transfer resistance (Ohm.cm^2)	Protection efficiency τ (%)	Porosity ratio (%)
Uncoated steel	**-765**	**2.8*10^3**	-----	-----
APPJ Pretreated steel	**-692**	**3.1*10^3**	**~1**	-----
ppHMDSO	**-695**	**0.7*10^6**	**99.57**	**0.423**
GN@ppHMDSO	**-687**	**5.6*10^7**	**99.94**	**0.050**
GN@ppHMDSO sandwich	**-701**	**7.1*10^8**	**99.99**	**0.004**

The results confirm that adding graphene sheets in the polymer matrix increases the charge transfer resistance thus the protection efficiency of the coatings. This can be explained by a decrease of the active surface of the pores in the coating which leads to a significant decrease in the corrosion rate.

Anticorrosion protection of GN@ppHMDSO hybrid coating

The corrosion-protection mechanism of GN@ppHMDSO hybrid layers developed by plasma

at atmospheric pressure can be explained according to three important critical steps as shown in Fig.10 (1) The surface activation with APPJ in air creates a stable iron oxide passivation layer (*i.e* Fe_2O_3 and FeO) which is essential to insure the adhesion of the coating to the substrate and therefore avoid or limit its delamination. The adhesion of the organosilicon layer to the substrate is probably achieved via the Fe-O-Si bindings. (2) The ppHMDSO matrix acts as a physical barrier to protect the metallic surface from the corrosive media. Nevertheless the polymer coating alone can contain pores and/or structure defects which will favour its swelling. (3) The structure of the graphene sheets offers an additional barrier layer to the diffusion of the ions in a corrosive media and reinforces the anticorrosion performance of nanocomposite GN@ppHMDSO coatings [50].

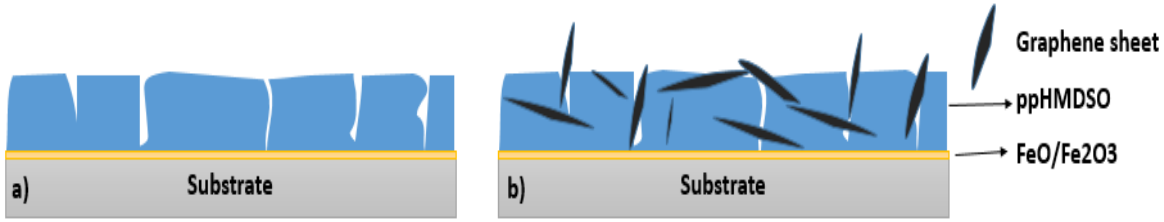

Fig.10: **a) ppHMDSO** **b) GN@ppHMDSO**

4. Conclusion

In summary, GN@ppHMDSO hybrid coatings were successfully developed by atomizing, a well-dispersed, stable colloidal suspension of graphene nanosheets and HMDSO precursor into a DBD plasma reactor at atmospheric pressure. We have shown that a small amount of around 1 wt% of GNs incorporated into HMDSO matrix does not modify the chemical composition of the ppHMDSO layer. We report also that the GN@ppHMDSO hybrid coatings showed a significant improved anticorrosion resistance to the corrosive media as compared to ppHMDSO coating alone. These results can be probably explained by the fact that owing to their homogenous dispersion into the polymer matrix, graphene nanosheets can play

a critical role as an additional physical barrier which will increase the diffusion path of the ions from the corrosive media inside the hybrid coatings.

Acknowledgement

A. Anagri would like to acknowledge Sorbonne Université for his PhD fellowship**.**

References

[1] Ramezanzadeh B, Haeri Z, Ramezanzadeh M. A facile route of making silica nanoparticles-covered graphene oxide nanohybrids (SiO2-GO); fabrication of SiO2-GO/epoxy composite coating with superior barrier and corrosion protection performance. Chemical Engineering Journal 2016;303:511–528.
[2] Yu Z, Di H, Ma Y, He Y, Liang L, Lv L, et al. Preparation of graphene oxide modified by titanium dioxide to enhance the anti-corrosion performance of epoxy coatings. Surface and Coatings Technology 2015;276:471–478.
[3] Chang K-C, Hsu M-H, Lu H-I, Lai M-C, Liu P-J, Hsu C-H, et al. Room-temperature cured hydrophobic epoxy/graphene composites as corrosion inhibitor for cold-rolled steel. Carbon 2014;66:144–153.
[4] Šest E, Dražič G, Genorio B, Jerman I. Graphene nanoplatelets as an anticorrosion additive for solar absorber coatings. Solar Energy Materials and Solar Cells 2018;176:19–29.
[5] Qi K, Sun Y, Duan H, Guo X. A corrosion-protective coating based on a solution-processable polymer-grafted graphene oxide nanocomposite. Corrosion Science 2015;98:500–506.
[6] Wu Q, Gong L-X, Li Y, Cao C-F, Tang L-C, Wu L, et al. Efficient flame detection and early warning sensors on combustible materials using hierarchical graphene oxide/silicone coatings. ACS Nano 2017;12:416–424.
[7] Xu H, Li Y, Huang N-J, Yu Z-R, Wang P-H, Zhang Z-H, et al. Temperature-triggered sensitive resistance transition of graphene oxide wide-ribbons wrapped sponge for fire ultrafast detecting and early warning. Journal of Hazardous Materials 2019;363:286–294.
[8] Qiang F, Hu L-L, Gong L-X, Zhao L, Li S-N, Tang L-C. Facile synthesis of super-hydrophobic, electrically conductive and mechanically flexible functionalized graphene nanoribbon/polyurethane sponge for efficient oil/water separation at static and dynamic states. Chemical Engineering Journal 2018;334:2154–2166.
[9] Angelini E, d'Agostino R, Fracassi F, Grassini S, Rosalbino F. Surface analysis of PECVD organosilicon films for corrosion protection of steel substrates. Surface and Interface Analysis: An International Journal Devoted to the Development and Application of Techniques for the Analysis of Surfaces, Interfaces and Thin Films 2002;34:155–159.
[10] Schreiber HP, Wertheimer MR, Wrobel AM. Corrosion protection by plasma-polymerized coatings. Thin Solid Films 1980;72:487–494.
[11] Bour J, Bardon J, Aubriet H, Del Frari D, Verheyde B, Dams R, et al. Different Ways to Plasma-Polymerize HMDSO in DBD Configuration at Atmospheric Pressure for Corrosion Protection. Plasma Processes and Polymers 2008;5:788–796.
[12] Fracassi F, d'Agostino R, Palumbo F, Angelini E, Grassini S, Rosalbino F. Application of plasma deposited organosilicon thin films for the corrosion protection of metals. Surface and Coatings Technology 2003;174:107–111.

[13] Petit-Etienne C, Tatoulian M, Mabille I, Sutter E, Arefi-Khonsari F. Deposition of SiOχ-Like Thin Films from a Mixture of HMDSO and Oxygen by Low Pressure and DBD Discharges to Improve the Corrosion Behaviour of Steel. Plasma Processes and Polymers 2007;4:S562–S567.
[14] Lommatzsch U, Ihde J. Plasma Polymerization of HMDSO with an Atmospheric Pressure Plasma Jet for Corrosion Protection of Aluminum and Low-Adhesion Surfaces. Plasma Processes and Polymers 2009;6:642–648.
[15] Vassallo E, Cremona A, Laguardia L, Mesto E. Preparation of plasma-polymerized SiOx-like thin films from a mixture of hexamethyldisiloxane and oxygen to improve the corrosion behaviour. Surface and Coatings Technology 2006;200:3035–3040.
[16] Benıtez F, Martınez E, Esteve J. Improvement of hardness in plasma polymerized hexamethyldisiloxane coatings by silica-like surface modification. Thin Solid Films 2000;377:109–114.
[17] Voevodin NN, Balbyshev VN, Khobaib M, Donley MS. Nanostructured coatings approach for corrosion protection. Progress in Organic Coatings 2003;47:416–423.
[18] Bardon J, Bour J, Del Frari D, Arnoult C, Ruch D. Dispersion of Cerium-Based Nanoparticles in an Organosilicon Plasma Polymerized Coating: Effect on Corrosion Protection. Plasma Processes and Polymers 2009;6:S655–S659.
[19] Dembele A, Rahman M, Reid I, Twomey B, MacElroy JM, Dowling DP. Deposition of hybrid organic–inorganic composite coatings using an atmospheric plasma jet system. Journal of Nanoscience and Nanotechnology 2011;11:8730–8737.
[20] Uygun A, Oksuz L, Yavuz AG, Guleç A, Sen S. Characteristics of nanocomposite films deposited by atmospheric pressure uniform RF glow plasma. Current Applied Physics 2011;11:250–254.
[21] Liguori A, Traldi E, Toccaceli E, Laurita R, Pollicino A, Focarete ML, et al. Co-Deposition of Plasma-Polymerized Polyacrylic Acid and Silver Nanoparticles for the Production of Nanocomposite Coatings Using a Non-Equilibrium Atmospheric Pressure Plasma Jet. Plasma Processes and Polymers 2016;13:623–632.
[22] Prasai D, Tuberquia JC, Harl RR, Jennings GK, Bolotin KI. Graphene: corrosion-inhibiting coating. ACS Nano 2012;6:1102–1108.
[23] Yu Y-H, Lin Y-Y, Lin C-H, Chan C-C, Huang Y-C. High-performance polystyrene/graphene-based nanocomposites with excellent anti-corrosion properties. Polymer Chemistry 2014;5:535–550.
[24] Ramezanzadeh B, Niroumandrad S, Ahmadi A, Mahdavian M, Moghadam MM. Enhancement of barrier and corrosion protection performance of an epoxy coating through wet transfer of amino functionalized graphene oxide. Corrosion Science 2016;103:283–304.
[25] Pourhashem S, Vaezi MR, Rashidi A, Bagherzadeh MR. Exploring corrosion protection properties of solvent based epoxy-graphene oxide nanocomposite coatings on mild steel. Corrosion Science 2017;115:78–92.
[26] Chang C-H, Huang T-C, Peng C-W, Yeh T-C, Lu H-I, Hung W-I, et al. Novel anticorrosion coatings prepared from polyaniline/graphene composites. Carbon 2012;50:5044–5051.
[27] Ramezanzadeh B, Ahmadi A, Mahdavian M. Enhancement of the corrosion protection performance and cathodic delamination resistance of epoxy coating through treatment of steel substrate by a novel nanometric sol-gel based silane composite film filled with functionalized graphene oxide nanosheets. Corrosion Science 2016;109:182–205.
[28] Fiche-Technique-Acier-S235JR(2).pdf n.d.

[29] Ben Said S, Arefi-Khonsari F, Pulpytel J. Plasma Polymerization of 3-Aminopropyltrietoxysilane (APTES) by Open-Air Atmospheric Arc Plasma Jet for In-Line Treatments. Plasma Processes and Polymers 2016;13:1025–1035.
[30] Naudé N, Cambronne JP, Gherardi N, Massines F. Electrical model and analysis of the transition from an atmospheric pressure Townsend discharge to a filamentary discharge. Journal of Physics D: Applied Physics 2005;38:530.
[31] Massines F, Sarra-Bournet C, Fanelli F, Naudé N, Gherardi N. Atmospheric pressure low temperature direct plasma technology: status and challenges for thin film deposition. Plasma Processes and Polymers 2012;9:1041–1073.
[32] Grundmeier G, Stratmann M. Influence of oxygen and argon plasma treatments on the chemical structure and redox state of oxide covered iron. Applied Surface Science 1999;141:43–56.
[33] Ozcan O, Pohl K, Keil P, Grundmeier G. Effect of hydrogen and oxygen plasma treatments on the electrical and electrochemical properties of zinc oxide nanorod films on zinc substrates. Electrochemistry Communications 2011;13:837–839.
[34] Yasuda HK. Plasma polymerization. Academic press; 2012.
[35] Rau C, Kulisch W. Mechanisms of plasma polymerization of various silico-organic monomers. Thin Solid Films 1994;249:28–37.
[36] Bour J, Charles L, Petersen J, Michel M, Bardon J, Ruch D. Insights in molecular structure of organosilicon plasma polymer produced by means of atmospheric pressure dielectric barrier discharge process. Plasma Processes and Polymers 2010;7:687–694.
[37] O'Hare L-A, Parbhoo B, Leadley SR. Development of a methodology for XPS curve-fitting of the Si 2p core level of siloxane materials. Surface and Interface Analysis: An International Journal Devoted to the Development and Application of Techniques for the Analysis of Surfaces, Interfaces and Thin Films 2004;36:1427–1434.
[38] O'Hare L-A, Hynes A, Alexander MR. A methodology for curve-fitting of the XPS Si 2p core level from thin siloxane coatings. Surface and Interface Analysis: An International Journal Devoted to the Development and Application of Techniques for the Analysis of Surfaces, Interfaces and Thin Films 2007;39:926–936.
[39] Grill A, Neumayer DA. Structure of low dielectric constant to extreme low dielectric constant SiCOH films: Fourier transform infrared spectroscopy characterization. Journal of Applied Physics 2003;94:6697–707. doi:10.1063/1.1618358.
[40] Kim CY, Kim SH, Kim HS, Navamathavan R, Choi CK. Formation mechanism and structural characteristics of low-dielectric-constant SiOC (-H) films deposited by using plasma-enhanced chemical-vapor deposition with DMDMS and O2 Precursors. Journal of Korean Physical Society 2007;50:1119.
[41] Jiang J-W, Tang H, Wang B-S, Su Z-B. Raman and infrared properties and layer dependence of the phonon dispersions in multilayered graphene. Physical Review B 2008;77. doi:10.1103/PhysRevB.77.235421.
[42] Ferrari AC, Meyer JC, Scardaci V, Casiraghi C, Lazzeri M, Mauri F, et al. Raman Spectrum of Graphene and Graphene Layers. Physical Review Letters 2006;97. doi:10.1103/PhysRevLett.97.187401.
[43] Sun G, Grundmeier G. Surface-enhanced Raman spectroscopy of the growth of ultra-thin organosilicon plasma polymers on nanoporous Ag/SiO2-bilayer films. Thin Solid Films 2006;515:1266–74. doi:10.1016/j.tsf.2006.03.027.
[44] Ghosh A, Rao KV, George SJ, Rao CNR. Noncovalent Functionalization, Exfoliation, and Solubilization of Graphene in Water by Employing a Fluorescent Coronene Carboxylate. Chemistry-A European Journal 2010;16:2700–4. doi:10.1002/chem.200902828.

[45] Mansfeld F. Use of electrochemical impedance spectroscopy for the study of corrosion protection by polymer coatings. Journal of Applied Electrochemistry 1995;25:187–202.
[46] Orazem ME, Tribollet B. Electrochemical impedance spectroscopy. John Wiley & Sons; 2017.
[47] Elsener B, Rota A, Bohni H. Impedance study on the corrosion of PVD and CVD titanium nitride coating. Mater. Sci. Forum, 44/45(1989), 29
[48] Barres T, Tribollet B, Stephan O, Montigaud H, Boinet M, Cohin Y. Characterization of the porosity of silicon nitride thin layer by Electrochemical Impedance Spectroscopy. Electrochimica Acta 227(2017) 1-6
[49] Fakhr Nabavi H, Aliofkhazraei M. Morphology, composition and electrochemical properties of bioactive-TiO2/HA on CP-Ti and Ti6Al4V substrates fabricated by alcali treatment of hybrid plasma electrolytic oxidation process (estimation of porosity from EIS results). Surface & Coatings Technology 375(2019) 266-291
[50] Ding R, Li W, Wang X, Gui T, Li B, Han P, et al. A brief review of corrosion protective films and coatings based on graphene and graphene oxide. Journal of Alloys and Compounds 2018;764:1039–55. doi:10.1016/j.jallcom.2018.06.133.